02

Investigation of the optical properties of a $BiFeO_3/SrTiO_3$ heterostructure grown on an $Al_2O_3(0001)$ substrate by RF cathode sputtering

© S.V. Kara-Murza[1], K.M. Zhidel[2], N.V. Korchikova[1], A.G. Silcheva[1], Yu.V. Tekhtelev[1], R.G. Chizhov[1], A.V. Pavlenko[2,3,*]

[1] Lugansk State Pedagogical University,
91011 Lugansk, Luhansk People's Republic
[2] Scientific Research Institute of Physics, Southern Federal University,
344090 Rostov-on-Don, Russia
[3] Southern Scientific Center, Russian Academy of Sciences,
344006 Rostov-on-Don, Russia

*e-mail: antvpr@mail.ru

Received April 7, 2022
Revised April 7, 2022
Accepted April 17, 2022

The phase composition, structure, and optical properties of the $BiFeO_3/SrTiO_3/Al_2O_3$ (c-cut) heterostructure have been studied using XRD analysis, spectrophotometry, and multi-angle ellipsometry. BFO/STO/Al_2O_3 heterostructures have been obtained by high-frequency cathode sputtering in an oxygen atmosphere using the intermittent deposition technology. It was found that the $BiFeO_3$ and $SrTiO_3$ layers grew with an orientation in the direction of the [111] crystallographic axis parallel to the normal to the Al_2O_3 substrate. It has been shown that the damaged layer on the surface of the heterostructure does not exceed 2–3 nm, and no signs of the presence of boundary layers at the $Al_2O_3-SrTiO_3$ and $SrTiO_3-BiFeO_3$ interfaces have been identified. The dispersion dependences of the refractive indices of BFO and STO layers are calculated. The reasons for the revealed regularities are discussed.

Keywords: thin films, multiferroic, optical properties, ellipsometry, bismuth ferrite.

DOI: 10.21883/EOS.2022.07.54724.3512-22

Introduction

Bismuth ferrite $BiFeO_3$ (BFO) is a multiferroic material that exhibits both magnetic and ferroelectric properties. Specifically, temperature T_C of the ferroelectric phase transition is 1103 K, and $T_N = 643$ K [1] corresponds to the antiferromagnetic phase transition. These high T_C and T_N values made BFO one of the most thoroughly studied multiferroic materials [1,2] with potential applications in multi-purpose environmentally friendly electronic devices with low power consumption [3]. It is known that thin $BiFeO_3$ film feature strong ferroelectric polarization ($P_r \sim 100\,\mu C/cm^2$) that exceeds the corresponding values for single-crystal samples [4]. The application potential of BFO-based nanostructures spurred the interest in examination of their properties and methods of fabrication [5]. The structure of BFO films is closely related to their epitaxial deformation in the process of growth on various substrates. The majority of studies focused on BFO films are performed on strontium titanate $SrTiO_3$ (001) (STO) substrates. A film is subjected to compressive stress on such substrates, and the tetragonal phase is established as a result. The BFO film thickness plays a crucial role: when it increases, elastic stress is relieved owing to the formation of a more stable R-like BFO phase, which is typical of large thicknesses. Ultrathin BFO films grown on (001) $SrTiO_3$ substrates with a $SrRuO_3$ buffer layer revealed the signs of transition to the tetragonal symmetry [6]. It was noted in [7] that BFO films grown on (001) $SrTiO_3$ substrates may feature a tetragonal structure with a giant c/a ratio, which is attributable to the emergence of a Bi_2O_3 layer forming between a film and a substrate. In general, the research data on dependences of the properties of BFO films on their thickness and the material of substrates and buffer layers still remain incomplete.

A detailed analysis of the surface morphology and the structural parameters of thin BFO films is necessary for their practical application. Specifically, the optical characteristics of BFO films are important for the development of optoelectronic devices, since their electrooptic, magnetooptic, and thermooptic properties may be adjusted by modulating the refraction index [8]. Without question, further studies of thin BFO films both on crystalline strontium titanate substrates and with this material used as a buffer layer are theoretically and practically relevant. In the present study, we report the results of examination of the structure, the phase composition, and the optical properties of the BFO/STO/Al_2O_3 (0001) heterostructure.

Methods of fabrication and examination of samples

Gas-discharge RF sputtering of BFO and STO films onto an Al_2O_3 substrate prepared in advance for heteroepitaxial deposition (C-plane; the substrate had a thickness of 0.43 mm and was fabricated by „MONOCRYSTAL“in Stavropol) was performed using a Plazma 50-SE setup. The phase composition, the structural perfection of films, and the lattice cell parameters were determined by X-ray diffraction using a „RIKOR“ multi-function X-ray unit ($Cu_{K\alpha}$ radiation).

The optical properties of films were examined by spectrophotometry and ellipsometry. The transmission spectrum was measured at room temperature in the 450–900 nm wavelength range with a Shimadzu UV-2450 spectrophotometer (the short-wavelength limit was established by the fundamental absorption in the Al_2O_3 substrate). Ellipsometric measurements were performed using a multi-angle reflective null ellipsometer at the helium–neon laser wavelength (632.8 nm). Ellipsometric angles Ψ and Δ, which specify the variation of parameters of the polarization ellipse in reflection of elliptically polarized light off the surface of a solid [9–11], were calculated based on the measured azimuths of the polarizer in the input ellipsometer arm and the analyzer in the output arm.

Experimental results and discussion

Only the reflections from planes (111) of BFO and STO layers were present in the $\theta-2\theta$ XRD patterns (Fig. 1). This is indicative of the lack of impurity phases and the fact that BFO and STO layers grow with a preferred orientation along the [111] crystallographic axis, which is parallel to the normal to the substrate (axis [006] of the Al_2O_3 substrate). The lattice cell parameters of BFO ($c = 0.3989$ nm) and STO ($c = 0.3955$ nm) were determined based on the (111) reflections maxima.

Figure 2 presents the optical transmission spectrum of the BFO/STO/Al_2O_3 structure. Low values of the transmission coefficient of this transparent heterostructure are attributable to dull finishing of the free substrate surface. Since the interference extrema are not related to the transmission coefficient value, a model of the substrate as an infinite medium was used in analysis [9]. The geometry of the system (Fig. 3) is as follows: *1* — air, *2* — $BiFeO_3$ film with thickness d_2 and refraction index n_2, *3* — $SrTiO_3$ layer with thickness $d_3 \ll d_2$ and refraction index n_3, *4* — substrate material with refraction index n_4. The transmission coefficient of the system with an exact geometry may be presented as

$$T = \frac{T_0}{1 - A\cos\delta_2 + B\cos\delta_3 - C\cos(\delta_2 + \delta_3)}, \qquad (1)$$

where $T_0 = n_4(t_{12}t_{23}t_{34})^2$, $A = |r_{12}r_{23}|$, $B = |r_{23}r_{34})|$, $C = |r_{12}r_{34}|$ (t_{ik} and r_{ik} — are the corresponding amplitude

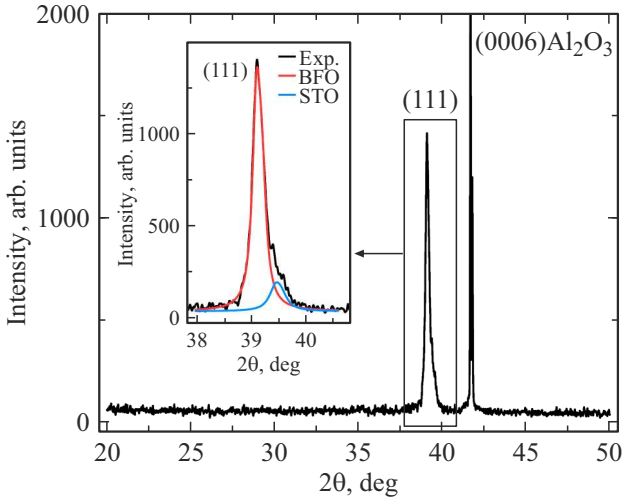

Figure 1. $\theta-2\theta$-XRD pattern of heterostructure BFO/STO/Al_2O_3.

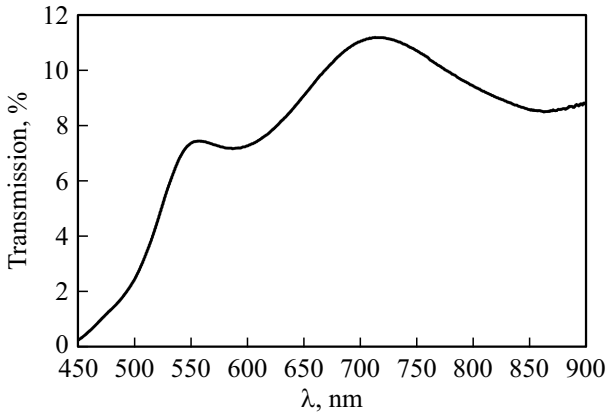

Figure 2. Transmission spectrum of heterostructure BFO/STO/Al_2O_3.

Fresnel transmission and reflection coefficients); only the terms of the order of smallness no higher than 2 were retained in the denominator of (1). The phase incursions in layers are

$$\delta_2 = \frac{4\pi}{\lambda} n_2 d_2, \qquad \delta_3 = \frac{4\pi}{\lambda} n_3 d_3, \qquad (2)$$

where $\delta_3 \ll \delta_2$. Since function $|\cos\delta_3|$ increases monotonically with wavelength, the interference extrema in the transparency region of the film are related to the first and the third terms of the function:

$$F(\lambda) = -A\cos\delta_2 + B\cos\delta_3 - C\cos(\delta_2 + \delta_3), \qquad (3)$$

where $\delta_2 = \delta_2^{(0)} + 2\pi m$ (m — is the interference order).

In addition to interference extrema, an optical transmission maximum may be observed in the transparency region at $\cos\delta_3 < 0$ and under the condition

$$A\cos\delta_2^{(0)} + C\cos\left(\delta_2^{(0)} + \delta_3\right) = 0. \qquad (4)$$

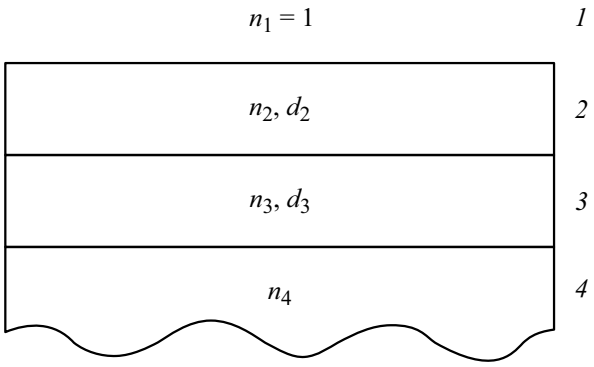

Figure 3. Optical model of heterostructure BFO/STO/Al_2O_3.

This condition, in turn, may be satisfied at certain ratios of coefficients A and C (between refraction indices n_2, n_3, n_4) if $\delta_2^{(0)}$ lies in the third quadrant and $\left(\delta_2^{(0)} + \delta_3\right)$ lies in the fourth quadrant (or $\delta_2^{(0)}$ and $\left(\delta_2^{(0)} + \delta_3\right)$ lie in the first and the second quadrants, respectively). The solving of Eq. (4) with two unknown quantities $\delta_2^{(0)}$ and $\left(\delta_2^{(0)} + \delta_3\right)$ then comes down to plotting a nomogram at the corresponding wavelength in these variables with subsequent selection of a pair of solutions satisfying the specified conditions. The results of analysis of the transmission spectrum features (Fig. 2) suggested that condition (4) is satisfied in the transparency region and the short-wave maximum of a modest height is attributable to term $B\cos\delta_3$ in (1)–(3), which corresponds to the buffer layer with $0.5\pi < \delta_3 < \pi$.

Tabulated values of refraction indices of layer and substrate materials were used to estimate the thickness of the BFO film and the buffer STO layer. The order of interference in the heterostructure was determined based on the nature of variation of equivalent phase thickness $(nd)_{eCV} = n_2d_2 + n_3d_3$ with increasing wavelength: it was found that $m = 2$ corresponds to the long-wave maximum at $\lambda = 712$ nm. The thickness of the buffer STO layer ($d_3 \sim 35$ nm) and, consequently, the BFO film thickness ($d_2 \sim 326$ nm) were estimated using the above-mentioned method based on the maximum transmission at wavelength $\lambda = 556$ nm.

Revised values of layer thicknesses and refraction indices were derived from ellipsometric measurement data [9,10]. The measurement results were processed with optimization methods [9–11] with an error below 1%.

Figure 4 presents the experimental (points) and calculated (curves) dependences of ellipsometric angles Ψ and Δ on incidence angle φ of probing radiation. The end results of ellipsometry are $n_2 = 3$, $d_2 = 324$ nm, $n_3 = 2.4$, $d_3 = 37$ nm, and $n_4 = 1.728$. These results suggest that boundary layers at Al_2O_3–$SrTiO_3$ and $SrTiO_3$–$BiFeO_3$ interfaces are lacking, and the thickness of the damaged layer on the free structure surface does not exceed 2–3 nm. The latter fact is indicative of a fairly high film quality.

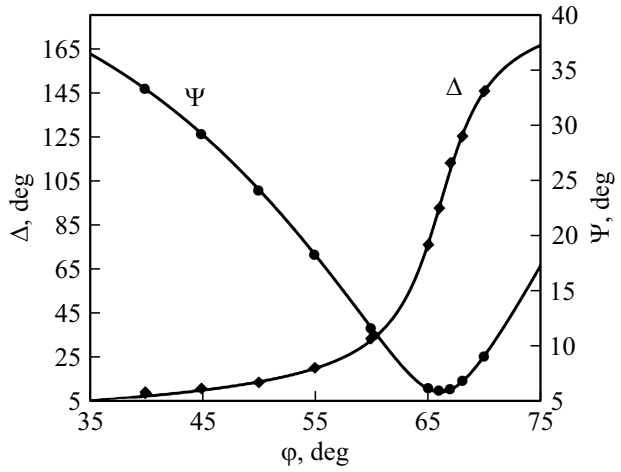

Figure 4. Calculated (solid curves) and experimental (points) dependences of ellipsometric angles Ψ and Δ on the incidence angle for heterostructure BFO/STO/Al_2O_3.

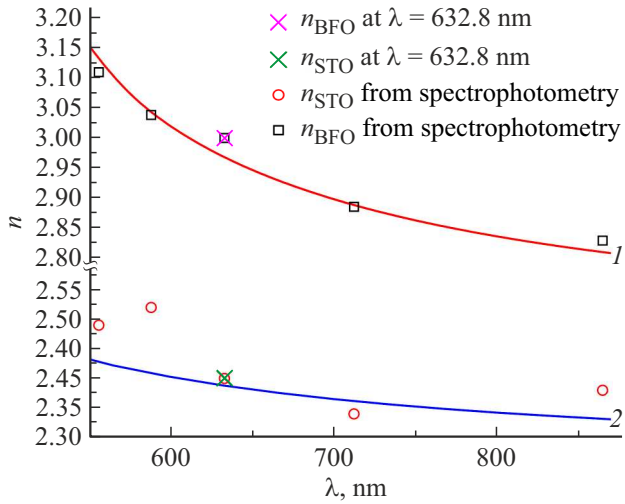

Figure 5. Spectral dependences of the refraction index of BFO and STO layers in heterostructure BFO/STO/Al_2O_3. Curves *1* and *2* represent $n(\lambda)$ for BFO and STO single crystals.

Dispersion characteristic of the refraction indices of BFO and STO derived from spectrophotometry and multi-angle ellipsometry data

λ, nm	556	588	632.8	712	864
$BiFeO_3$					
n	3.109	3.038	3.00	2.886	2.83
$SrTiO_3$					
n	2.49	2.52	2.40	2.34	2.38

The spectrometry and ellipsometry data were used to determine the dispersion characteristic of the refraction indices of the BFO film and the buffer STO layer (see the table and Fig. 5). It can be seen that the refraction indices

of the BFO film derived from spectrometry and multi-angle ellipsometry data ($\lambda = 632.8$ nm) agree fairly well with the corresponding values for the bulk material. At the same time, a considerable scatter of the refraction index values for the buffer STO layer is evident. The smallness of the number of experimental spectrophotometry points may be a contributing factor here, but the results of a preliminary spectral ellipsometry analysis of the optical properties of this heterostructure in the 550–900 nm range („ELLIPS-1991“ellipsometer) suggest that the obtained results are correct.

Conclusions

1. The method of gas-discharge RF cathode sputtering in oxygen atmosphere was used to fabricate BFO(111)/STO(111)/Al_2O_3(0001) heterostructures with lattice cell parameters $c_{BFO} = 0.3989$ nm, $c_{STO} = 0.3955$ nm. No impurity phases were revealed by X-ray diffraction analysis and optical examination.

2. Extrema of the optical transmission spectrum of the BFO/STO heterostructure were examined by spectrophotometry. It was found that a short-wave maximum of a moderate height is attributable to the buffer STO layer; the thickness of STO and BFO layers was estimated.

3. Multi-angle ellipsometry at the wavelength of a helium–neon laser (632.8 nm) made it possible to determine accurately the thicknesses of layers ($d_{BFO} = 324$ nm, $d_{STO} = 37$ nm) and their refraction indices ($n_{BFO} = 3.0$, $n_{STO} = 2.4$). Boundary Al_2O_3–$SrTiO_3$, $SrTiO_3$–$BiFeO_3$ layers were not found. The thickness of the damaged layer on the heterostructure surface does not exceed 2–3 nm.

4. Accurate values of the layer thickness derived from ellipsometry data provided an opportunity to determine the dispersion characteristics of refraction indices of BFO and STO layers.

Acknowledgments

Equipment provided by the „Joint Center of Research and Processing Equipment of the Southern Scientific Center of the Russian Academy of Sciences (Research, Development, Practical Evaluation)“ and „Electromagnetic, Electromechanical, and Thermal Properties of Solids“ (Research Institute of Physics, Southern Federal University) common use centers was used in this study. The authors wish to thank Cand. Sci. (Phys.–Math.), senior staff scientist D.V. Stryukov for his help in interpreting the X-ray data.

Funding

This study was supported financially by the Ministry of Science and Higher Education of the Russian Federation (state research assignment, scientific project No. (0852-2020-0032)/(BAZ0110/20-3-07IF)).

Conflict of interest

The authors declare that they have no conflict of interest.

References

[1] N. Wang, X. Luo, L. Han, Z. Zhang, R. Zhang, H. Olin, Y. Yang. Nano-Micro Lett., **12**, 81 (2020). DOI: 10.1007/s40820-020-00420-6
[2] G. Catalan, J.F. Scott. Adv. Mater., **21**, 2463 (2009). DOI: 10.1002/adma.200802849
[3] S. Seki, X.Z. Yu, S. Ishiwata, Y. Tokura. Science, **336**, 198 (2012). DOI: 10.1126/science.1214143
[4] J. Wang, J.B. Neaton, H. Zheng, V. Nagarajan, S.B. Ogale, B. Liu, D. Viehland, V. Vaithyanathan, D.G. Schlom, U.V. Waghmare, N.A. Spaldin, K.M. Rabe, M. Wuttigand, R. Ramesh. Science, **299**, 1719 (2003). DOI: 10.1126/science.1080615
[5] M.H. Lee, D.J. Kim, J.S. Park, S.W. Kim, T.K. Song, M.-H. Kim, W.-J. Kim, D. Do, I.-K. Jeong. Adv. Mater., **27**, 6976 (2015). DOI: 10.1002/adma.201502424
[6] Y. Yang, C.M. Schlepuetz, C. Adamo, D.G. Schlom, R. Clarke. APL Mater., **1**, 052102 (2013). DOI: 10.1063/1.4827596
[7] H. Liu, P. Yang, K. Yao, J. Wang. Appl. Phys. Lett., **98**, 102902 (2011). DOI: 10.1063/1.3561757
[8] H. Shima, K. Tsutsumi, M. Suzuki, T. Tadokoro, H. Naganuma, S. Okamura, T. Kamei. Jpn. J. Appl. Phys., **57** (11S) 11UF10 (2018). DOI: 10.7567/jjap.57.11uf10
[9] K.M. Zhidel, S.V. Kara-Murza, N.V. Korchikova, Yu.V. Tekhtelev, A.V. Pavlenko, L.I. Kiseleva. J. Adv. Dielectr., **3** (1), 260014 (2020). DOI: 10.1142/S2010135X21600146
[10] V.A. Gritskikh, I.V. Zhikharev, S.V. Kara-Murza, N.V. Korchikova, Yu.M. Nikolaenko, A.A. Tikhii. in *Trudy 7-go mezhdunarodnogo simpoziuma „Fizika poverkhnostnykh yavlenii, mezhfaznykh granits i fazovye perekhody“* (Fond Nauki Obraz., 2017), Vol. 7, p. 53 (in Russian).
[11] A.A. Tikhii, V.A. Gritskikh, S.V. Kara-Murza, Yu.M. Nikolaenko, V.V. Faraponov, I.V. Zhikharev. Opt. Spectrosc., **119** (2), 268 (2015). DOI: 10.7868/S0030403415080231